

STUDY OF THE X-RAY ACTIVITY OF SGR A* DURING THE 2011 XMM-NEWTON CAMPAIGN

Enmanuelle Mossoux¹, Nicolas Grosso¹, Fr ed eric H. Vincent² and Delphine Porquet¹

Abstract. Sgr A* is the closest supermassive black hole ($\sim 4 \times 10^6 M_{\odot}$) located at the dynamical center of our galaxy. It has a very low bolometric luminosity ($\sim 9.4 \times 10^{-9}$ times the Eddington luminosity) and, consequently, a very low mass accretion rate ($\sim 10^{-6} M_{\odot}/\text{yr}$) but flaring activity can be observed in near-infrared, X-ray, sub-millimeter and radio. To constrain the origin of such events, it is important to investigate the timing and spectral properties of these flares, especially in X-rays. During the 2011 XMM-Newton campaign (whose total exposure was ~ 226 ks) in coordination with the 1.3 mm Very-Long-Baseline Interferometry array, two X-ray flares have been observed in the 2 – 10 keV energy band. To perform the timing analysis of the light curves, we apply the Bayesian-blocks method to the XMM-Newton event lists, using a two-step algorithm to correct for any detector flaring background. Furthermore, we compute X-ray smoothed light curves in order to have better accuracy on the substructures and the amplitude of the flares. The first X-ray flare was observed on March 30, 2011 with a peak amplitude of about 3 times the non-flaring level. It is characterized by two sub-flares: the first one is very short (~ 458 s) with an unabsorbed peak-luminosity of $\sim 9.4 \times 10^{34}$ erg s⁻¹, whereas the second one is longer (~ 1542 s) with a lower unabsorbed peak-luminosity ($\sim 6.8 \times 10^{34}$ erg s⁻¹). The waiting time between the two sub-flares (~ 1000 s) is one of the smallest ever observed. If we compare this value with those observed during the 2012 Chandra XVP campaign, we can favor the hypothesis that this event is a single flare rather than two distinct sub-flares. We developed a hotspot model to explain the double-peaks shape of the light curve of this flare with the gravitational lensing and Doppler boosting. However, the decrease of the flux back to the quiescent level between the two substructures cannot be satisfactorily reproduced with this simple model. This observation allows us to reject this flaring model even when it is made slightly more complex than a simple hotspot. The very rapid flux variation during the first sub-flare allow us to constrain the distance and the size of the flaring source. Since the proper time around a supermassive black hole is always longer than the observed duration due to the time dilatation in strong gravity field and assuming that the rise and decay phases are due to magnetic energy heating and synchrotron cooling of infrared photons, respectively, we derive a range to the radial distance of 4 – 100(+19, -29) rg with $\text{rg}=0.04$ AU. The corresponding source radii at this distance are $1.8 - 2.87 \pm 0.01$ rg.

Keywords: Galaxy: center, X-rays: Sgr A*, radiation mechanisms: general

1 Introduction

Our Galaxy hosts Sgr A* the closest supermassive black hole at a distance of about 8 kpc (Genzel et al. 2010; Falcke & Markoff 2013). It has a mass $M_{\text{BH}} = 4 \times 10^6 M_{\odot}$ (Sch odel et al. 2002; Ghez et al. 2008; Gillessen et al. 2009) and is usually in a steady state, emitting predominately at radio to submillimeter wavelengths. The detections of flares from Sgr A* have provided a valuable way to scrutinize accreting matter close to the event horizon. The X-ray flare frequency is 1.1 (1.0-1.3) flare per day with $L_{2-8 \text{ keV}} \geq 10^{34}$ erg s⁻¹ (Neilsen et al. 2013). The bulk of X-ray flares detected so far have faint-to-moderate amplitudes (Baganoff et al. 2003; Neilsen et al. 2013), and three very bright flares have been observed to share very similar spectral properties (Porquet et al. 2003, 2008; Nowak et al. 2012). When near-infrared (NIR) and X-ray flares are detected simultaneously, their light curves have similar shapes, and there is no apparent delay (< 3 min) between the peaks of flare

¹ Observatoire Astronomique de Strasbourg, Universit e de Strasbourg, CNRS, UMR 7550, 11 rue de l'Universit e, F-67000 Strasbourg, France.

² Nicolaus Copernicus Astronomical Center, ul. Bartycka 18, 00-716 Warszawa, Poland.

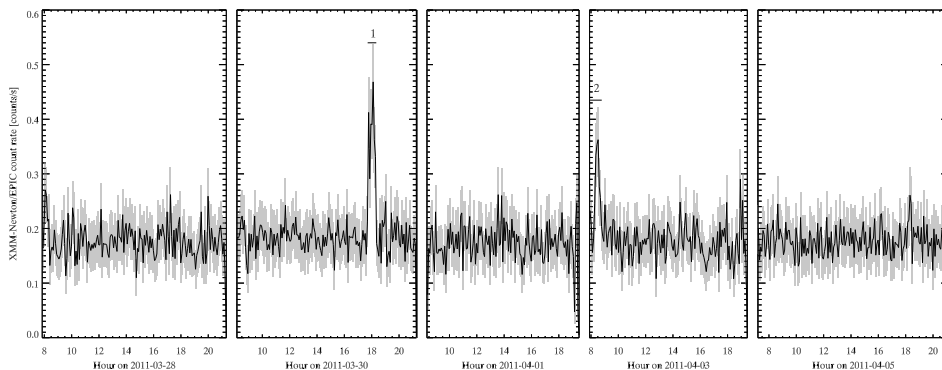


Fig. 1. pn+MOS1+MOS2 light curves of Sgr A* in the 2–10 keV energy range binned on 300 s. The X-ray flares are labeled from 1 to 2. The horizontal lines below these labels are the flare durations.

emission (e.g., Yusef-Zadeh et al. 2006; Dodds-Eden et al. 2009; Eckart et al. 2012). The current interpretation is that both X-ray/NIR flares come from a region close to the event horizon, while delayed sub-mm (e.g., ≈ 100 min; Marrone et al. 2008) and mm peaks (up to 5 hours; Yusef-Zadeh et al. 2009) have been interpreted as the adiabatic cooling of an expanding relativistic plasma blob. While NIR flares are known to be due to synchrotron emission (Eisenhauer et al. 2005; Eckart et al. 2006), the X-ray flare emission mechanism has not been settled yet, with arguments for synchrotron (Dodds-Eden et al. 2009; Barrière et al. 2014), inverse Compton (Yusef-Zadeh et al. 2012), and synchrotron self-Compton (Eckart et al. 2008) models.

We report here the results published in Mossoux et al. (2015a,b) of the 2011 XMM-Newton campaign for Sgr A* observation.

2 XMM-Newton observations: data processing and timing analysis

The 2011 observational campaign of Sgr A* with XMM-Newton (AO-8, 5×33 ks; PI: D. Porquet) was scheduled on 2011 Mar. 28 and 30 and Apr. 1, 3, and 5 for a total effective exposure of ≈ 226 ks. The data were reduced using the Science Analysis Software (SAS) package (v.13.5 and CCF of 04/04/2014) and filtered in the 2–10 keV energy range. The pn on-axis Half Energy Width is $\approx 20''$ at 1.5 keV (Ghizzardi 2002). To extract the events coming from Sgr A*, we thus define the source+background (src+bkg) region as a $10''$ -radius disk around the VLBI radio position of Sgr A* (Reid et al. 1999). For each observation and detector, we first built the src+bkg and the bkg (extracted from a $3' \times 3'$ region on the same CCD) light curves. After applying relative corrections, we create the bkg-subtracted light curves. Finally, the light curves of the three detectors were summed to produce the total light curve shown in Fig. 1.

To identify the flaring and non-flaring levels under a certain probability using the *unbinned* event arrival time, we used the Bayesian blocks analysis proposed by Scargle (1998) and improved by Scargle et al. (2013a). This recursive algorithm performs a segmentation of the event list into blocks with statistically different count-rates levels. The time defining two successive blocks is called a change point. To use this algorithm, we have to calibrate the prior estimate of the number of change points to the false detection probability ($p = e^{-3.5}$; Neilsen et al. 2013; Nowak et al. 2012) and the number of points in the observation. We also correct the blocks count rate from the observation time lost during the CCD read out and we reject the time where the camera did not observe. The blocks count rate is also corrected from the background count rate by applying successively the Bayesian blocks algorithm on the bkg and src+bkg region and then applying the algorithm on the src+bkg region with a weight adjusting the Voronoi time-interval in order to subtract the average background (Scargle et al. 2013b). The non-flaring level is defined as the count rate of the longest block and the flaring levels are the highest blocks. This algorithm gives us the duration of the flaring and non-flaring levels with better accuracy than in a binned light curve since it uses the best temporal resolution available. Moreover, it has a better detection efficiency compared to previous methods which only detect a flare if its peak on the binned light curve is higher than 3 times the standard deviation of the non-flaring light curve. The Bayesian blocks analysis is applied independently on each cameras. The non flaring level is about $0.18 \text{ count s}^{-1}$ during all observations which is consistent with the one previously observed with XMM-Newton (e.g., in 2007, Porquet et al. 2008). Two X-ray flares are detected on 2011 Mar. 30 and Apr. 3.

To improve the characterization of the amplitude and the time of a local maximum or minimum, we compute a smoothed light curve by applying a density estimator (Silverman 1986; Feigelson & Babu 2012) on the *unbinned* event arrival times. We use the Epanechnikov kernel (inverse parabola shape) with a window width of the kernel

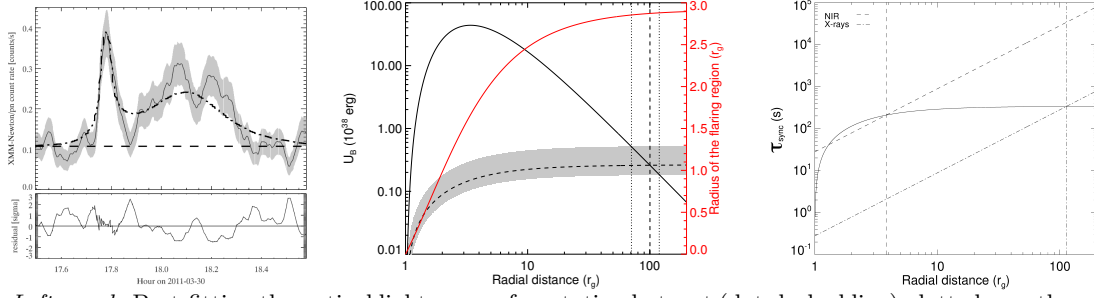


Fig. 2. *Left panel:* Best-fitting theoretical light curve of a rotating hotspot (dot-dashed line) plotted over the pn smoothed light curve (solid line, with 1σ error in gray) of the 2011 Mar. 30 flare. The non-flaring level is the horizontal dashed line. The lower panel gives the residual in units of the standard deviation of the binned light curve. *Middle panel:* Magnetic energy vs. radial distance. The solid line is the distribution of the magnetic energy (left y-axis). The dashed line and gray band are the flare total energy and its errors with 90% confidence level, respectively. The vertical lines are the upper limits to the distance. The red line is the radius of the emitting region (right y-axis). *Right panel:* Synchrotron cooling time vs. radial distance. The solid line is $\Delta\tau_{\text{decay}}(r)$. The vertical lines are the lower limits to the radial distance.

of 100 s since it is defined on a finite support which allows us to control any boundary effects. The density estimator is also corrected from the background count rate by applying the same weight than for the Bayesian blocks analysis. The error of the smoothed light curve is assumed to be Poissonian. The smoothed light curve of the first flare is superimposed to the binned light curve in Fig. 2 (left panel). This flare has 211 ± 25 counts and an amplitude of 0.284 ± 0.013 count s^{-1} (computed using the smoothed light curve). It is characterized by two components: a short (~ 458 s) and symmetrical subflare and a longer (~ 1542 s) and fainter symmetrical subflare separated by only ~ 1000 s. Between these two subflares, the smoothed light curve returns to a level consistent with the non-flaring state during less than 100 s. The second flare has more than 154 ± 24 counts and an amplitude of 0.165 ± 0.012 count s^{-1} .

3 Gravitational lensing of a hotspot-like structure

We modeled the two subflares of the 2011 Mar. 30 flare with a single mechanism since its shape could be the signature of a gravitational lensing of a hotspot-like structure: the primary maximum is the gravitational lensing of the light emitted by the hotspot when it is on the opposite side of the black hole with respect to the observer whereas the secondary maximum is the relativistic beaming of the light emitted when the source is moving toward the observer. The hotspot has a spherical and optically thin structure in solid rotation around the black hole with Keplerian angular velocity and its emitted spectrum is assumed to follow a power law. Maps of the observed spectrum were computed by using the open-source ray-tracing code GYOTO (Vincent et al. 2011). The light curve is obtained by summing each of these maps over all pixels and solid angle to compute a flux. Our hotspot model is defined by three physical parameters: the orbital radius r , the hotspot radius R and the black hole inclination i . The spin parameter has a low impact on the light curve, thus it is fixed to $a = 0.99$. The left panel of Fig. 2 shows the best fit that is found for the following values: $r = 12r_g$, $R = 1.4r_g$, $i = 86.5^\circ$ with $r_g = 0.04$ au the gravitational radius ($\chi_{\text{red}}^2 = 0.85$). This figure clearly shows that the local minimum of the light curve, in between the two bumps at around 17.53 h, is not well fit by the hotspot model. This inadequacy is sufficient to reject this simple model without adding some ad hoc new components since a hotspot-like model will always produce a local minimum at a higher level than the non-flaring level.

4 Constraining the radial distance of the first 2011 Mar. 30 subflare

We consider that the short duration of the rise phase of the first subflare ($\Delta t_{\text{rise}} = 115$ s) places a limit to the size of the flaring region (e.g., Dodds-Eden et al. 2009). We compute the proper-to-observed time ratio ($\Delta\tau(r) > \Delta t$) due to time dilation in strong gravity field.

We constrain the radius of the spherical flaring region by considering that the Alfvén velocity cannot be higher than the speed of light (Dodds-Eden et al. 2009): $R < c\Delta\tau_{\text{rise}}$. This leads to an upper limit on the volume V of the flaring region used to compute the magnetic energy: $U_B = \frac{B^2 V}{8\pi}$ with $B = B_{1R_S} 2r_g/r$ the magnetic field vs. the radial distance r (see Barrière et al. 2014, and references therein). The average luminosity of the first subflare is $L_{2-10 \text{ keV}}^{\text{unabs}}(\text{flare}) = 5.8_{-1.7}^{+5.7} \times 10^{34}$ erg s^{-1} . If we assume a maximum efficiency, the upper limit to the radial distance is obtained from the balance between the flare total energy and the magnetic energy. The result is $r < 100_{-29}^{+19} r_g$ and the corresponding radius of the flaring region at this distance is $R = 2.87 \pm 0.01 r_g$

(see Fig. 2, middle panel).

The electrons that are accelerated by the release of the magnetic energy cool by emitting synchrotron radiation with the following timescale: $\tau_{\text{sync}} = 8 (B/30 \text{ G})^{-3/2} (\nu/10^{14} \text{ Hz})^{-1/2} \text{ min}$ (Dodds-Eden et al. 2009). This synchrotron cooling timescale must be equal to the decay time of the first subflare. If the X-ray photons are the primary source of synchrotron cooling, we derive $r > 114 r_g$, which is not consistent with the previously derived upper limit since sustained heating must also be present during the decay phase. Thus, we consider the synchrotron cooling time of NIR photons which leads to $r > 4 r_g$ with the flaring region outside the event horizon.

5 Conclusions

We have reported the data analysis of the XMM-Newton 2011 campaign for the observation of Sgr A*. We used the Bayesian-blocks algorithm and a density estimator applied on the unbinned event arrival time to constrain the duration, the position, and the amplitude of the X-ray flares with better accuracy. We observed two X-ray flares: on 2011 Mar. 30 and Apr. 03. The first flare is composed of two subflares: a very short-duration one and a longer and less luminous one. We modeled its two subflares with a single physical phenomenon using the gravitational lensing of a hotspot-like structure. However, the consistency of the observed flux level between the two subflare peaks with the non-flaring level led us to conclude that the light curve of this X-ray flare cannot satisfactorily be reproduced by a gravitational lensing event. Using the short duration of the first 2011 Mar. 30 subflare, we conclude that $4 r_g < r < 100_{-29}^{+19} r_g$ in this subflare for $B_{1R_s} = 100 \text{ G}$. The corresponding radii of the flaring region at these distances are $1.8 r_g < R < 2.87 \pm 0.01 r_g$.

References

- Baganoff, F. K., Maeda, Y., Morris, M., et al. 2003, *ApJ*, 591, 891
 Barrière, N. M., Tomsick, J. A., Baganoff, F. K., et al. 2014, *ApJ*, 786, 46
 Dodds-Eden, K., Porquet, D., Trap, G., et al. 2009, *ApJ*, 698, 676
 Eckart, A., Baganoff, F. K., Schödel, R., et al. 2006, *A&A*, 450, 535
 Eckart, A., García-Marín, M., Vogel, S. N., et al. 2012, *A&A*, 537, A52
 Eckart, A., Schödel, R., García-Marín, M., et al. 2008, *A&A*, 492, 337
 Eisenhauer, F., Genzel, R., Alexander, T., et al. 2005, *ApJ*, 628, 246
 Falcke, H. & Markoff, S. B. 2013, *Classical and Quantum Gravity*, 30, 244003
 Feigelson, E. D. & Babu, G. J. 2012, *Modern statistical method for astronomy with R applications*, ed. Cambridge University Press (Cambridge, UK)
 Genzel, R., Eisenhauer, F., & Gillessen, S. 2010, *Reviews of Modern Physics*, 82, 3121
 Ghez, A. M., Salim, S., Weinberg, N. N., et al. 2008, *ApJ*, 689, 1044
 Ghizzardi, S. 2002, In flight calibration of the PSF for the pn camera (EPIC-MCT-TN-012), Tech. rep.
 Gillessen, S., Eisenhauer, F., Fritz, T. K., et al. 2009, *ApJ*, 707, L114
 Marrone, D. P., Baganoff, F. K., Morris, M. R., et al. 2008, *ApJ*, 682, 373
 Mossoux, E., Grosso, N., Vincent, F. H., & Porquet, D. 2015a, *A&A*, 573, A46
 Mossoux, E., Grosso, N., Vincent, F. H., & Porquet, D. 2015b, *A&A*, 580, C2
 Neilsen, J., Nowak, M. A., Gammie, C., et al. 2013, *ApJ*, 774, 42
 Nowak, M. A., Neilsen, J., Markoff, S. B., et al. 2012, *ApJ*, 759, 95
 Porquet, D., Grosso, N., Predehl, P., et al. 2008, *A&A*, 488, 549
 Porquet, D., Predehl, P., Aschenbach, B., et al. 2003, *A&A*, 407, L17
 Reid, M. J., Readhead, A. C. S., Vermeulen, R. C., & Treuhaft, R. N. 1999, *ApJ*, 524, 816
 Scargle, J. D. 1998, *ApJ*, 504, 405
 Scargle, J. D., Norris, J. P., Jackson, B., & Chiang, J. 2013a, *ApJ*, 764, 167
 Scargle, J. D., Norris, J. P., Jackson, B., & Chiang, J. 2013b, 2012 Fermi Symp. Proc. – eConf C121028 [arXiv:1304.2818v1]
 Schödel, R., Ott, T., Genzel, R., et al. 2002, *Nature*, 419, 694
 Silverman, B. W. 1986, *Density Estimation for Statistics and Data Analysis*, ed. C. . Hall (Chapman & Hall)
 Vincent, F. H., Paumard, T., Gourgoulhon, E., & Perrin, G. 2011, *Classical and Quantum Gravity*, 28, 225011
 Yusef-Zadeh, F., Bushouse, H., Wardle, M., et al. 2009, *ApJ*, 706, 348
 Yusef-Zadeh, F., Roberts, D., Wardle, M., Heinke, C. O., & Bower, G. C. 2006, *ApJ*, 650, 189
 Yusef-Zadeh, F., Wardle, M., Dodds-Eden, K., et al. 2012, *AJ*, 144, 1